ACS OMEGA

http://pubs.acs.org/journal/acsodf

Article

Alginate-Stabilized Gold Nanoparticles Prepared Using the Microwave-Induced Plasma-in-Liquid Process with Long-Term Storage Stability for Potential Biomedical Applications

Haoran Liu, Kai Ikeda, Mai Thanh Nguyen, Susumu Sato, Naoki Matsuda, Hiroki Tsukamoto, Tomoharu Tokunaga, and Tetsu Yonezawa*

Cite This: *ACS Omega* 2022, 7, 6238–6247

Read Online

ACCESS | Metrics & More | Article Recommendations | Supporting Information

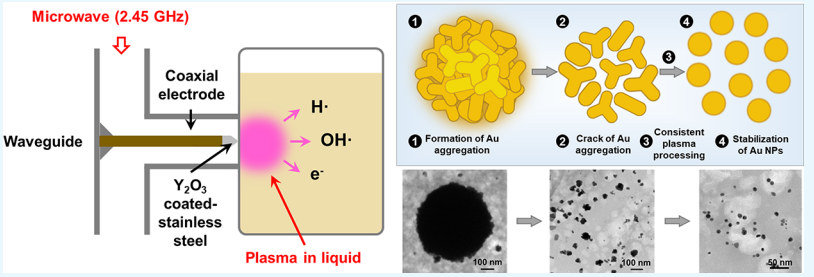

ABSTRACT: A one-step preparation of alginate-stabilized gold nanoparticles (Au NPs) using the microwave-induced plasma-in-liquid process (MWPLP) was reported. Effects of alginate with various concentrations on the preparation and properties of the synthesized Au NPs, including reaction rate, morphology, size, and optical absorption property, were studied. The introduction of alginate (1) accelerated the reaction rate, (2) prevented aggregation and precipitation due to long time discharge in MWPLP, and (3) provided long-term colloidal stability. An abnormal size change (from large to small) of Au NPs during particle growth, which was opposite to the typical change in bottom-up chemical reduction, was observed and a possible mechanism was proposed based on the dynamical and thermodynamical instability of particles during growth. The strategy of drying and redispersion of Au NPs in alginate solution was also studied. The drying and redispersion process had an imperceptible effect on the Au NPs. As a consequence, this strategy might be an effective technique for the long-term storage of Au NPs and other metal NPs. The alginate-stabilized Au NPs without the addition of toxic reducing or stabilizing agents can be appropriate to biomedical applications.

1. INTRODUCTION

Gold nanoparticles (Au NPs) are one of the most investigated nanomaterials that exhibit great potential in various biomedical applications, such as imaging, therapy, immunotherapy, drug delivery system, *etc.*[1] For example, the property of inducing a strong X-ray attenuation of gold makes Au NPs an ideal candidate for CT contrast agents.[2−4] The function design, such as surface modification with peptide,[5] enables the selective and sensitive targeting of the tumor while inducing a distinct contrast in CT imaging (increased X-ray attenuation).[6] Au NPs can also be imaged via terahertz microscopy by converting NIR light into heat.[7] Regarding therapeutic applications, Au NPs show great promise as photothermal therapeutic agents. This is because the surface plasmon resonance (SPR) of Au NPs can be designed by tailoring their size, shape, composition, and structure to absorb light in the NIR range in which minimum absorption by biological molecules, such as hemoglobin, and water is observed.[8] For drug delivery purposes, Au NPs could be conjugated to a variety of antitumor substances by simple physical adsorption or by using alkanethiol linkers.[9] For building a delivery system, target molecules (*e.g.*, cetuximab) can be applied along with the active substance to ensure better anchoring and penetration of the complex into the target cells.

Of all the methods for preparing Au NPs, chemical reduction is the most used strategy in which gold ions in a precursor are reduced by reducing agents such as ethanol,[10,11] polyol,[12] sodium borohydride,[13,14] β-D-glucose,[15] glycerol,[16] sodium citrate,[17] *etc.* On the other hand, to prevent the aggregation and flocculation of Au NPs in liquid, stabilizing agents such as poly(vinyl alcohol) or poly(vinyl pyrrolidone) are also used.[10,11,18] However, byproducts might be generated during reactions due to the introduction of reducing and stabilizing agents. These agents may also bring biological

Received: November 30, 2021
Accepted: February 1, 2022
Published: February 10, 2022

toxicity, and therefore, washing and water treatment are indispensable. In contrast, the plasma-in-liquid process represents a green alternative in NP synthesis.[18−25] Especially, the microwave-induced plasma-in-liquid (MWPLP) process is very interesting due to its relatively low energy consumption and no need for using toxic reducing and stabilizing agents (Scheme 1a).[18,22−26] In MWPLP, plasma is created in three

Scheme 1. (a) Experimental Setup of MWPLP for the Preparation of Au NPs; (b) Schematic Illustration of Microwave-Induced Plasma in the Reaction Vessel; (c) Fabrication Route for Preparing Au NPs in Aqueous Solutions of Sodium Alginate and $AuCl_4^-$

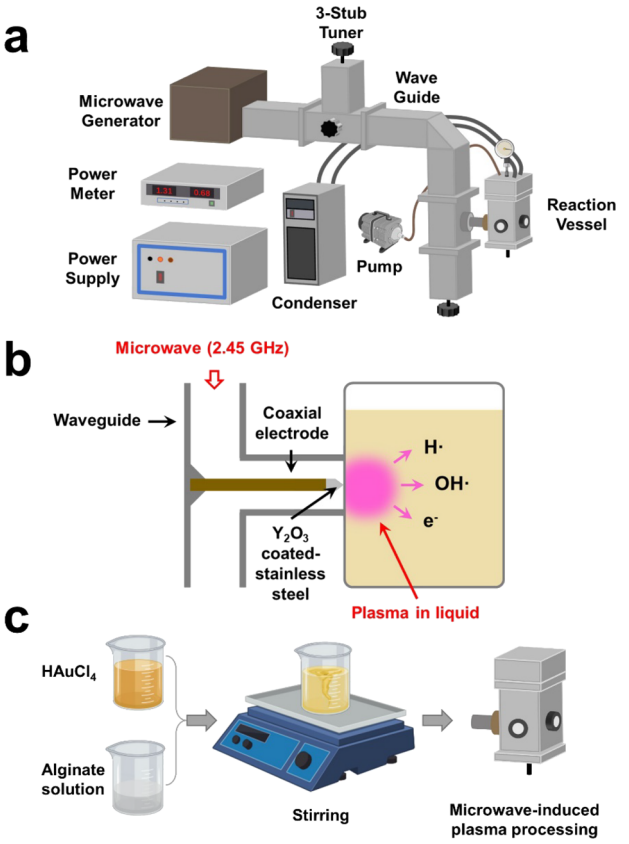

stages: (1) bubble formation, in which the liquid surrounding the electrode is heated by joule heating via microwaves, resulting in the outburst of bubbles;[27] (2) initiation of plasma, in which plasma is initiated toward the gas (provided by bubbles)/liquid interface; (3) formation of the plasma in liquid.[28] MWPLP is constituted based on a gas phase in a liquid phase. In our MWPLP apparatus (Scheme 1b), the plasma generated under low pressure can decompose water molecules to form highly reactive species, including hydrated electrons and hydrogen and hydroxyl radicals. Reaction equations for this process are summarized in eqs 1−4:

$$H_2O \rightarrow H\cdot + OH\cdot \quad (1)$$

$$M^{n+} + nH\cdot \rightarrow M + nH^+ \quad (2)$$

$$2OH\cdot \rightarrow H_2O_2 \quad (3)$$

$$M^{n+} + n/2H_2O_2 \rightarrow M + n/2O_2 + nH^+ \quad (4)$$

In these equations, M, H·, and OH· represent a metal, hydrogen radicals, and hydroxyl radicals, respectively. Water is decomposed by plasma to form hydrogen and hydroxyl radicals (eq 1). Then, hydrogen radicals reduce metal ions (eq 2). H_2O_2 generated based on the combination of hydroxyl radicals also reduces metal ions (eqs 3 and 4).[21] Although MWPLP can be used for the green synthesis of Au NPs, the challenges of the low reaction rate, excessive reaction-induced aggregation, and long-term stability of Au NPs still remain for further biomedical applications. Sodium alginate is a natural polymer with excellent biocompatibility, low toxicity, and mild gelation ability in divalent cation buffer. Alginate molecules can be dissolved in water because of negatively charged carboxyl groups. For an accelerated reaction and better stability, alginate was introduced in MWPLP (Scheme 1c). In the present work, the effects of sodium alginate on the preparation, morphology, size, and optical absorption property of Au NPs were studied. The proposed mechanism for the formation of Au NPs in alginate via MWPLP was demonstrated. Also, the strategy of drying and redispersion of Au NPs in alginate solution was studied and presented for the long-term storage of Au NPs and other metal NPs.

2. RESULTS AND DISCUSSION

2.1. UV−Vis Spectra of the Obtained Au NPs-Alginate Aqueous Dispersions. Figure 1 shows the UV−Vis extinction spectra of Au NPs prepared in pure water and sodium alginate aqueous solutions of different concentrations for various reaction times. The spectra of Au NPs prepared in pure water exhibited a surface plasmon resonance (SPR) peak with a maximum absorption wavelength (λ_{max}) at around 557 nm. The λ_{max} values of Au NPs prepared in alginate solution with concentrations of 0.5, 1.0, and 2.0% (w/v) were at 539, 554, and 573 nm, respectively. The peak intensities of these SPR peaks of Au NPs prepared in the solutions with different concentrations of sodium alginate did not change obviously, indicating that sodium alginate had no significant effect on the yield of Au NPs. The red shifts of λ_{max} (1.0 and 2.0% (w/v) groups) were caused by weak aggregation states of the adjacent Au NPs due to the surge in the number of Au NPs. As shown in Figure S1, after being diluted to the same sodium alginate concentration of 0.5% (w/v) group, the 1.0 and 2.0% (w/v) groups showed shorter λ_{max} (533 and 529 nm) than that of 0.5% (w/v) group (539 nm). For Au NPs prepared in pure water, it could be noted that the peak intensity reached a maximum at 20 min with the increase in reaction time. It suggests that the reaction from Au^{3+} to Au^0 would require approximately 20 min or more to complete. For Au NPs prepared in aqueous solutions of sodium alginate with various concentrations, all the absorption intensities of Au NPs reached the maximum value within 10 min, suggesting that the reaction could be completed within 10 min. These phenomena strongly suggest that the addition of sodium alginate could accelerate the reaction rate from Au^{3+} to Au^0. Furthermore, the absorption intensity of Au NPs prepared in pure water gradually decreased after reaching the maximum value, which was caused by the reduced concentration of Au NPs in dispersion due to the excessive MWPLP-induced aggregation and precipitation. Interestingly, the absorption intensities of Au NPs prepared in sodium alginate solutions were stable after reaching the maximum. The SPR peaks showed an ideal bell shape, which implies that negligible aggregation occurred, and the Au NPs are well dispersed in

https://doi.org/10.1021/acsomega.1c06769
ACS Omega 2022, 7, 6238−6247

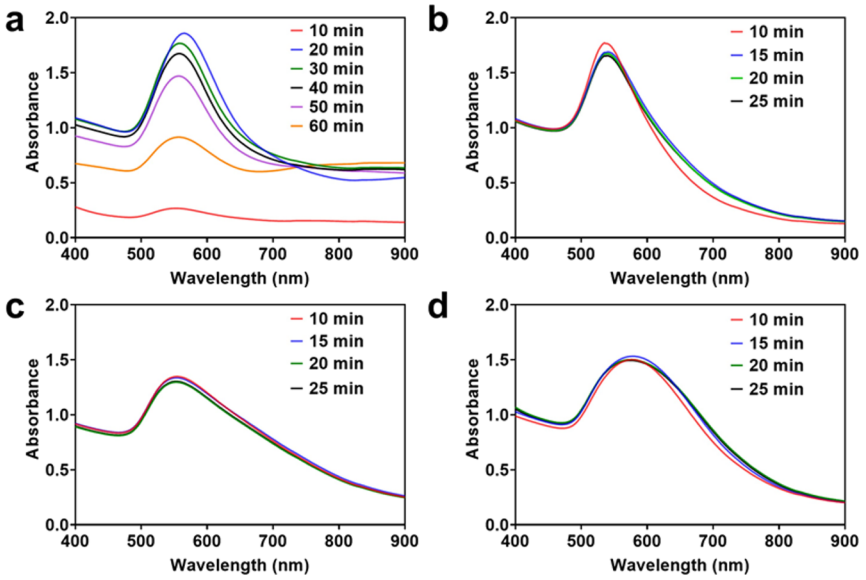

Figure 1. UV−Vis spectra of Au NP dispersions prepared in (a) pure water and aqueous solutions of sodium alginate with concentrations of (b) 0.5% (w/v), (c) 1.0% (w/v), and (d) 2.0% (w/v) for various reaction times.

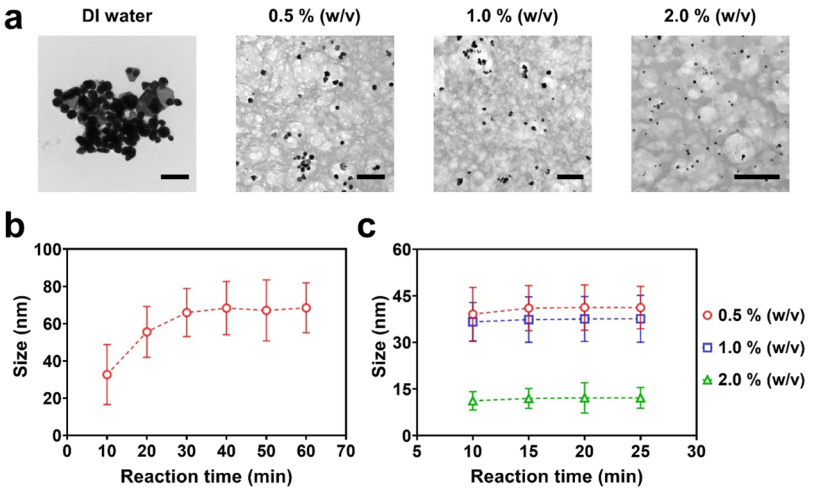

Figure 2. (a) TEM images of Au NPs prepared in pure water and sodium alginate aqueous solutions (reaction time: 20 min). Scale bars are 200 nm. (b) Average size of Au NPs prepared in pure water with different reaction times. (c) Average size of Au NPs prepared in alginate aqueous solution with different concentrations and reaction times.

dispersions. These results suggest that, in the presence of sodium alginate, Au NPs did not aggregate and precipitate due to the increase in reaction time, indicating that alginate can prevent the aggregation and precipitation caused by excessive MWPLP.

2.2. Effect of the Concentration of Sodium Alginate on the Morphology, Size, and Size Distribution of Au NPs. Transmission electron microscopy (TEM) images of Au NPs prepared in pure water and aqueous solutions of sodium alginate with different concentrations (reaction time: 20 min), along with their size distributions, are collected in Figure 2a and Figure S2. As shown in Figure 2a, the Au NPs prepared in pure water are mostly spherical, while a few show triangular and hexagonal shapes. It was previously reported that triangular and hexagonal particles were obtained from the preparation of Au NPs using the plasma-in-liquid process.[29] When they occurred on the surface of Au-nucleated seeds, reductions were dependent on the surface energy of the different crystal facets, and polygonal particles were generated.[18] In contrast, almost all the Au NPs prepared in sodium alginate solution showed spherical shapes. In addition, the Au NPs prepared in pure water contacted each other and showed a tendency to aggregate because these particles were naked (without coating of sodium alginate). After MWPLP in sodium alginate solutions, Au NPs were uniformly dispersed. Figure S3 shows the zeta potentials and pH values of Au NP dispersions. Zeta potentials of Au NP dispersions prepared in alginate (−40.60 to −55.17 mV) are more negative than that prepared in pure water (−10.80 mV). Therefore, the electrostatic repulsion of Au NPs prepared in pure water is weaker than the electrostatic and steric repulsion provided by $-COO^-$ groups of alginate chains.[30,31] Accordingly, the Au NPs prepared in pure water are more easily aggregated than that prepared in the presence of alginate. In Figure 2b, starting from 10 min, the particle size of the Au NPs prepared in pure water increased with increasing reaction time and reached a relatively stable value (around 68 nm) within 30 min. This is a result of the assembly and merging between Au NPs due to the lack of

https://doi.org/10.1021/acsomega.1c06769
ACS Omega 2022, 7, 6238−6247

Scheme 2. Illustration of the Formation Process of Alginate-Stabilized Au NPs

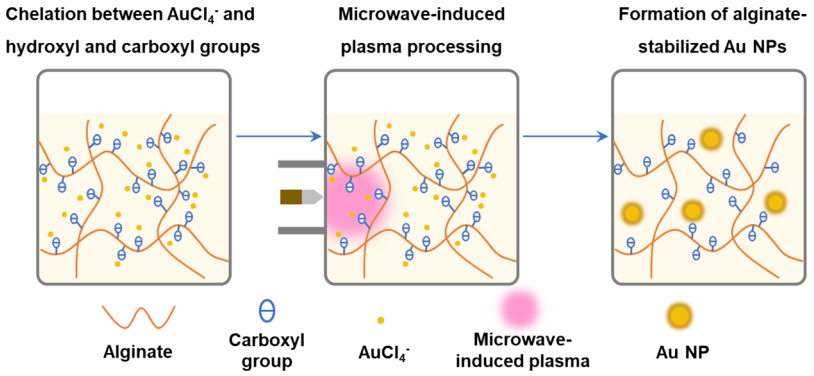

capping agents.[32,33] As the reaction time increased further, although the size stopped increasing, Au NPs started to aggregate and precipitate, as shown in Figure S4. Conversely, as illustrated in Scheme 2, after the addition of alginate, the chelation between gold chloride complexes and carboxyl and hydroxyl groups would allow gold ions to evenly disperse in solution.[34] After MWPLP, Au NPs could be generated in the alginate chain-formed cavities in situ. The formed Au NPs anchored strongly with the functional groups (−COO^- and −OH) of alginate. This helped prevent further assembly, merging, and aggregation of Au NPs.[30] The sizes of Au NPs were almost constant at different reaction times from 10 to 25 min, indicating that the reactions could be completed within 10 min with the assistance of alginate. At the same time, no aggregation and precipitation are observed in Figure S5, reflecting that the addition of alginate could indeed accelerate the reaction and prevent subsequent aggregation and precipitation caused by inordinate MWPLP. By comparing the sizes and size distributions of Au NPs produced in different concentrations of alginate solution in Figure 2c, the size of Au NPs gradually decreased with increasing alginate concentration. This is because alginate forms cavities and functions as a template for the growth of the Au NPs.[31] The alginate chains closer to each other in a higher concentration of alginate solution would form smaller cavities that could limit the uncontrollable growth of Au NPs. The size of Au NPs has a significant impact on their biomedical applications. For example, for all Au NPs with sizes ranging from 10 to 250 nm, the majority of gold was present in the liver and spleen.[35] A clear difference could be observed between the distribution of the 10 nm particles and the larger particles. The 10 nm particles are present in various organ systems including blood, liver, spleen, kidney, testis, thymus, heart, lung, and brain, whereas the larger particles can only be detected in blood, liver, and spleen. In addition, the size of Au NPs also affects their metabolism,[36] cytotoxicity,[37] and radiosensitization.[38] The sizes of Au NPs changed in a large range (from 41 to 12 nm) based on the concentration control of alginate solution (from 0.5 to 2.0% (w/v)). Therefore, the size of Au NPs can be controlled by tuning the concentrations of alginate solutions for broadening their applicability in a variety of biomedical applications.

2.3. Formation Mechanism of Au NPs Using MWPLP.

Alginate can accelerate the reaction and all reduction reactions can complete within 10 min, as evidenced by both results of UV−Vis spectra and the sizes of Au NPs prepared in alginate solutions in comparison with that in pure water. To investigate the formation of Au NPs during the initial stage of the reaction, Au NPs were collected at 1, 2, 3, 4, and 5 min with an alginate solution concentration of 2% (w/v) for characterizations. Figure 3a,b shows the TEM images and average sizes

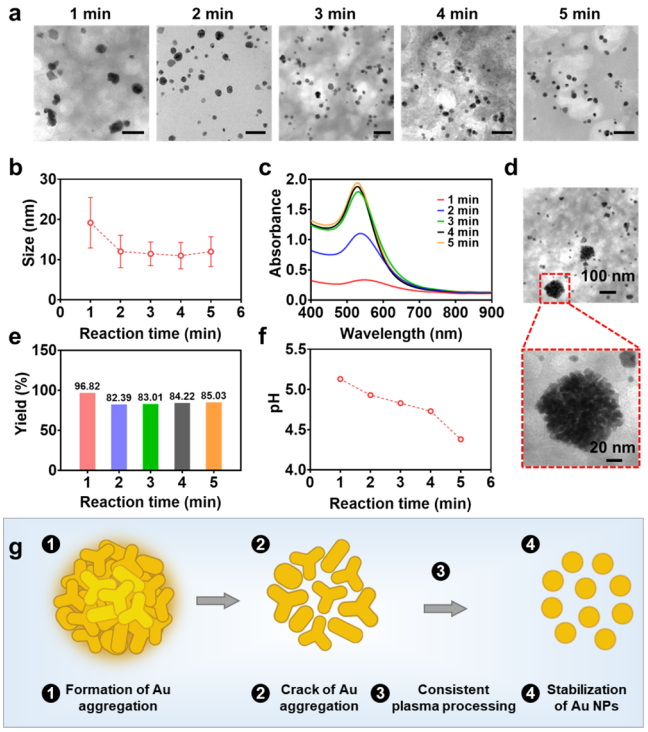

Figure 3. (a) TEM images of Au NPs prepared in alginate aqueous solutions (2.0% (w/v)) at different reaction times. Scale bars are 50 nm. (b) Average size of Au NPs prepared in alginate aqueous solutions (2.0% (w/v)) for different reaction times. (c) UV−Vis spectra of Au NPs prepared in alginate aqueous solutions (2.0% (w/v)) with different reaction times. (d) TEM images of Au aggregation with a reaction time of 1 min. (e) Yield of Au NPs prepared in alginate aqueous solutions (2.0% (w/v)) with different reaction times. (f) pH of Au NP dispersions with different reaction times. (g) Mechanism of Au NP formation using MWPLP.

of Au NPs prepared in alginate solutions (2.0% (w/v)) with different reaction times. It could be noted that differing from the Au NPs prepared in water with increasing size over time, the size of the Au NPs prepared in alginate solutions decreased in the first 5 min. In Figure 3c, the absorption intensity increases with reaction time, indicating that Au^{3+} was gradually transformed into Au^0. The blue shift of the SPR peak in the first 5 min of the reaction is a result of the breakdown of Au

https://doi.org/10.1021/acsomega.1c06769
ACS Omega 2022, 7, 6238−6247

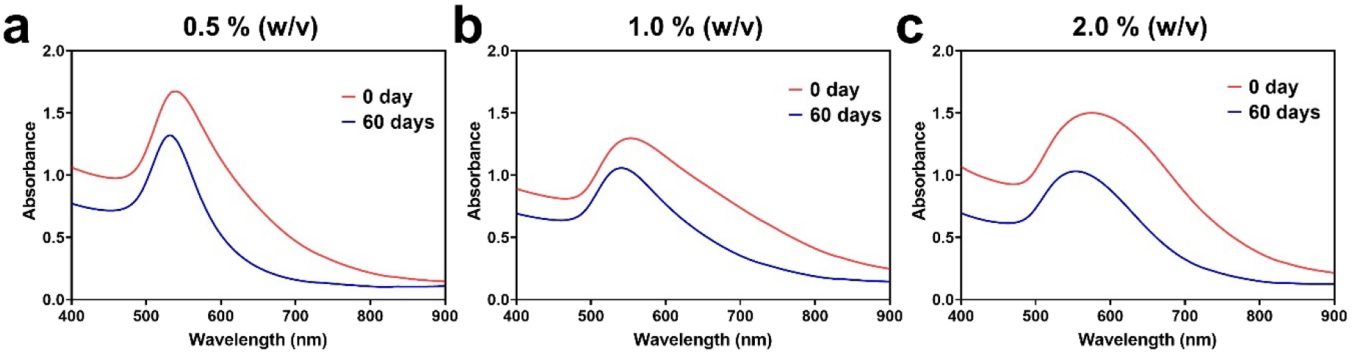

Figure 4. UV−Vis spectra of sodium alginate-stabilized Au NP dispersions at 0 day and 60 days after preparation with various sodium alginate concentrations: (a) 0.5% (w/v), (b) 1.0% (w/v), and (c) 2.0% (w/v).

NPs from their aggregation as found previously (Section 2.1) and observed in TEM. Interestingly, aggregations with a diameter of about 100−150 nm were found in the first minute, as shown in Figure 3d, and disappeared within 2 min. The EDS result suggests that the aggregation was Au^0 (Figure S6). At the same time, the yield of Au NPs (Figure 3e) calculated based on ICP data was 96.82% in the first minute, which means that 96% of Au^{3+} transformed into Au^0. The yield decreased and stabilized at around 85% after 2 min, suggesting that about 11% of Au^0 turned back into Au^{3+}. These results imply that Au NPs may be generated from large gold aggregations during the reaction. The XRD result (Figure S7) after 25 min reaction supported the presence of Au. Further, the size of Au NPs was gradually reduced due to dissolution under the decreasing pH condition during this process, as shown in Figure 3f. To validate this process, a low-concentration alginate solution (1.0% (w/v)) was used to appropriately slow down the reaction rate. TEM images (Figure S8) show that large-size aggregations also existed in the early stage of the reaction, and EDS confirmed the component of the aggregation (Figure S9). The size of Au NPs also decreased with increasing reaction time (Figure S10). Based on the results, a schematic diagram of the proposed formation mechanism of Au NPs is shown in Figure 3g. Briefly, alginate with the assistance of high temperature generated by MWPLP shows relatively strong reducibility[30,39] and results in a dynamical instability. The dynamical instability dramatically accelerates the transformation of Au^{3+} to Au^0 in a very short time and leads to the formation of Au atom aggregations. The Au atom aggregations are in a high-energy state because of the rapid reduction process. At the same time, alginate is an anionic polymer with high charge density, and the negatively charged alginate facilitates the attraction and crack of high-energy Au aggregations for lower energy.[30] After that, the Au atom aggregations crack into irregular Au NPs, and the reaction will continue with the presence of microwave-induced plasma and alginate. Also, the irregular Au NPs gradually become spherical NPs for thermodynamic stability.[40] However, due to the decrease in pH and the formation of cavities by alginate chains, which can function as a template for the Au NPs, the size of the Au NPs decreased and was gradually stabilized. The formation of Au NPs may therefore be composed of four steps: (1) formation of Au aggregation due to plasma-enhanced alginate reduction, (2) crack of Au aggregation for lower energy and higher stability, (3) consistent plasma processing, and (4) stabilization of Au NPs because of an alginate template.

2.4. Effect of Alginate on the Stability of Au NPs. Figure S11 shows images of Au NPs prepared in pure water on day 0, day 1, and day 7 and Au NPs prepared in alginate solutions with different concentrations on day 0 and day 60. It can be seen that the Au NPs prepared in water aggregated and precipitated after 1 day, while a part of Au NPs prepared in alginate solutions precipitated after 60 days and the rest suspended in alginate solution. Quick aggregation of Au NPs prepared in pure water is consistent with their small absolute zeta potential value (−10.80 mV, Figure S3a). Usually, NPs are considered stable if the zeta potential is more positive than +30 mV or more negative than −30 mV due to electrostatic repulsions.[25,41] As shown in Figure S3a, all Au NPs prepared in alginate solutions have zeta potentials more negative than −30 mV, which make them stable for much longer time compared with Au NPs in pure water. The aggregation degree of metal NPs could also be effectively reflected by changes in the absorption characteristics, especially the shift of the SPR peak in the UV−Vis spectra.[42,43] If strong aggregation occurred for Au NPs after a long storage period, a strong red shift of the SPR peak would be observed in the UV−Vis spectra.[30] As shown in Figure 4, after 60 days, the absorption intensity of Au NPs prepared in different concentrations of alginate decreased, indicating that the total amount of Au NPs in dispersions was reduced. Surprisingly, the blue shift, instead of red shift, of the SPR peak could be observed, suggesting that the size of Au NPs in the dispersions after 60 days was smaller than that of the samples on day 0. Therefore, it can be inferred that after 60 days of storage, mainly large-sized Au NPs precipitated, while small-sized Au NPs were still suspended in alginate solution. Compared with Au NPs prepared in pure water, the addition of alginate can stabilize small-sized NPs and slow down the precipitation rate of large-sized Au NPs.

2.5. Drying and Redispersion of Au NPs-Alginate Aqueous Dispersions. Keeping the stability of Au NPs is an important prerequisite for maintaining their designed functions and further biomedical applications. The low stability of Au NPs can complicate their use in biological environments, in particular, the formation of irreversible aggregations when they are subjected to physical and chemical changes (*e.g.*, contact with biofluids, freeze-drying, and ion strength gradients).[44] Further, the low stability also complicates various steps of the manufacturing and shipping processes.[45] Up to now, some compounds such as surfactants[46] or cyclodextrin[47] have been used to modify NPs to counter the challenge of instability.[48] Despite the advances made with those methods, the challenge remains in producing highly stable NPs and retaining the long-

https://doi.org/10.1021/acsomega.1c06769
ACS Omega 2022, 7, 6238−6247

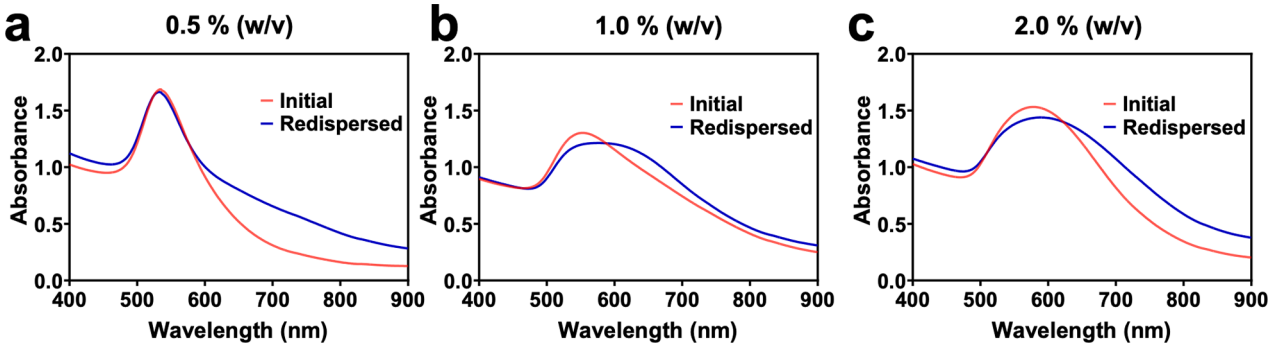

Figure 5. UV−Vis spectra of sodium alginate-stabilized Au NP dispersions before drying and after redispersion with various sodium alginate concentrations: (a) 0.5% (w/v), (b) 1.0% (w/v), and (c) 2.0% (w/v).

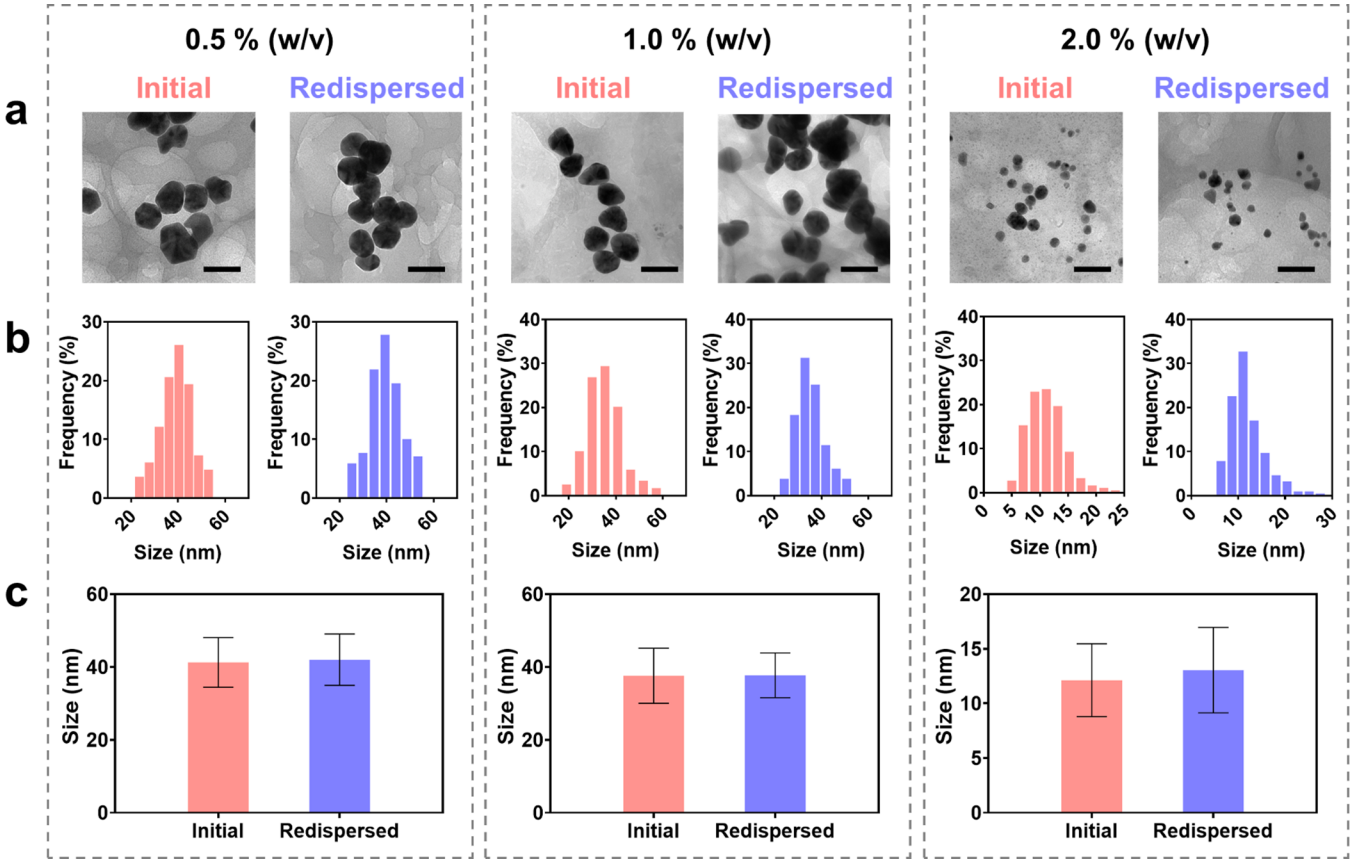

Figure 6. (a) TEM images, (b) size distributions, and (c) average sizes of Au NPs before drying and after redispersion with various sodium alginate concentrations. Scale bars, 50 nm.

term stability of functionalized NPs.[49] The strategy of drying and redispersion was therefore adopted to maintain the stability and dispersibility of Au NPs. This is based on the cavities formed by alginate chains that could function as a template and provide barriers to prevent Au NPs from contacting each other. From Figure 5, the UV−Vis spectrum results showed that there was no significant change in the absorption intensity after drying and redissolution, indicating that the concentration of Au NPs in dispersions did not decrease substantially. But the broadening of the SPR peak implies a slight aggregation of Au NPs. By observing and analyzing TEM images as shown in Figure 6a, it can be found that the shape and dispersion of Au NPs have not changed. From Figure 6b,c, there is no significant change in the size distributions and average sizes of Au NPs before drying and after redispersion. These results reveal that the Au NPs prepared in alginate solutions could aggregate slightly, but the morphology, dispersion, and size were not significantly affected after the drying and redispersion process. In addition, the intravenously injected NPs may be rapidly cleared from the body by the reticuloendothelial system (RES) and accelerated blood clearance phenomenon (ABC phenomenon), which affect the therapeutic effect significantly. For homogeneous distribution, long-term in situ retaining, and low leakage, the gelation ability of Au NPs suspended in alginate solution was studied before drying and after redispersion, as shown in Figure 7. All alginate solutions with different concentrations exhibited fluid-like behavior after injection in the buffer with a physiological concentration of Ca^{2+} (1.8 mM). With the increase in concentration to 3.6 mM, alginate-stabilized Au

https://doi.org/10.1021/acsomega.1c06769
ACS Omega 2022, 7, 6238−6247

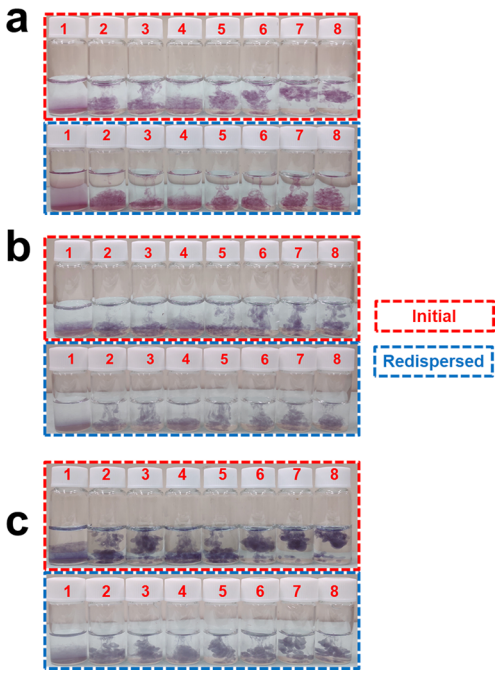

Figure 7. Gelation ability of sodium alginate solutions with concentrations of (a) 0.5% (w/v), (b) 1.0% (w/v), and (c) 2.0% (w/v) in Ca^{2+} buffer before drying (red) and after redispersion (blue). Ca^{2+} concentrations: #1: 1.8 mM; #2: 3.6 mM; #3: 5.4 mM; #4: 7.2 mM; #5: 9.0 mM; #6: 10.8 mM; #7: 12.6 mM; #8: 14.4 mM.

NPs rapidly transformed into gels, and the drying and redissolution process had no effect on the gelation ability of alginate solutions with different concentrations. Therefore, the addition of alginate could not only accelerate the reaction and prevent aggregation and precipitation but also improve the long-term storage stability of Au NPs and the convenience of storage or shipping process of a large amount of Au NPs compared with the Au NPs stored in liquid. The process of drying and redispersion with alginate as a stabilizing agent might also provide a new strategy for the long-term storage of other metal NPs.

2.6. Accelerated Stability Test of Alginate-Stabilized Au NPs. As defined by the International Council for Harmonization of Technical Requirements for Pharmaceuticals for Human Use (ICH), the accelerated stability test is designed to study the chemical degradation or physical change of a drug substance or drug product by using exaggerated storage conditions for predicting the expiration date or lifespan under the recommended storage conditions. To estimate the long-term stability, alginate-stabilized Au NPs were kept at 40 °C, which is the most commonly used accelerated stability storage condition for drug products within the USA market, for 1, 2, 3, and 4 month(s) to simulate the storage at 25 °C for 0.5, 1.0, 1.5, and 2.0 year(s). Figure 8 shows the UV−Vis spectrum results of alginate-stabilized Au NPs with different alginate concentrations; the negligible change in the absorption intensity with a broadening SPR peak implies that the amount of Au NPs nearly remained constant and a minor aggregation between Au NPs occurred. The shape and dispersion of alginate-stabilized Au NPs also did not change after being kept for 4 months, as evidenced by the TEM images shown in Figures S12−S14. Figure 9 shows that the average sizes of Au

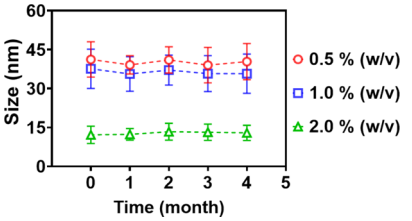

Figure 9. Average size of sodium alginate-stabilized Au NPs prepared with various sodium alginate concentrations after the accelerated stability test. Sodium alginate concentrations: red circle, 0.5% (w/v); blue square, 1.0% (w/v); green triangle, 2.0% (w/v).

NPs stabilized with various concentrations of alginate are almost the same after the accelerated stability test. In addition, after being dispersed in pure water, the alginate-stabilized Au NPs display an excellent injectability and gelation ability in Ca^{2+} buffer, as Figure 10 illustrates. In an extra experiment for

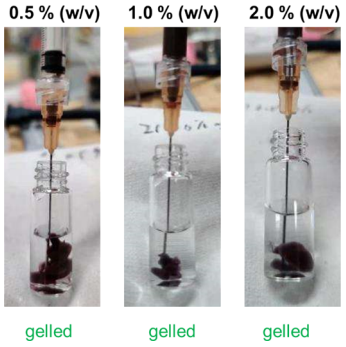

Figure 10. Injectability and gelation performance of sodium alginate-stabilized Au NPs in Ca^{2+} buffer (1.8 mM) after the accelerated stability test.

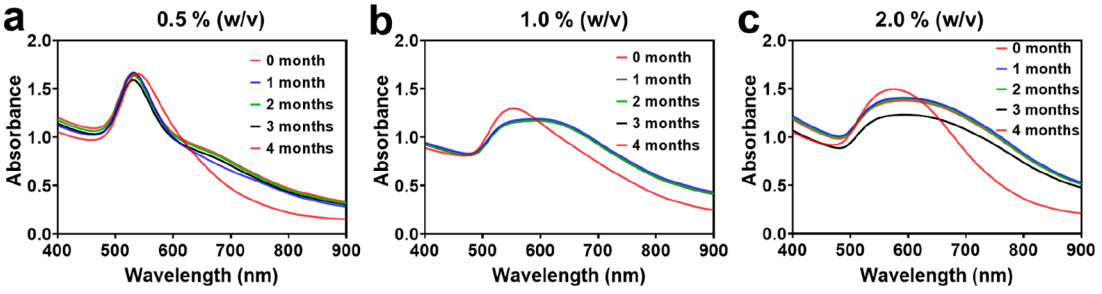

Figure 8. UV−Vis spectra of sodium alginate-stabilized Au NPs prepared with various sodium alginate concentrations ((a) 0.5% (w/v), (b) 1.0% (w/v), and (c) 2.0% (w/v)) after the accelerated stability test.

https://doi.org/10.1021/acsomega.1c06769
ACS Omega 2022, 7, 6238−6247

evaluating the universality of the drying and redispersion process on the stability of alginate-stabilized Au NPs after long-term storage, type I-1 alginate (molecular weight, 1.5×10^6) was substituted by type I-8 alginate with a higher molecular weight (molecular weight: 3.2×10^6). TEM (Figures S15–S17) shows that the I-8 alginate-stabilized Au NPs are spherical, suggesting that increasing molecular weight of alginate did not affect the morphology of Au NPs. However, smaller average sizes and narrower size distributions of Au NPs are correlated with the increase in the molecular weight of alginate (Figure 2c and Figures S15–S18). After being kept for 4 months, no apparent changes were observed in the UV–Vis spectra (Figure S19) and average sizes (Figure S18) of I-8 alginate-stabilized Au NPs. The redispersed I-8 alginate-stabilized Au NPs have a superb injectability and gelation ability as well (Figure S20). These results suggest the positive effect of alginate on the stability of Au NPs, ensuring their expected performance in practical applications within the designed lifespan. It is conceivable that the introduction of alginate and the subsequent drying and redispersion process could serve as a powerful tool for the long-term storage of metal NPs. The higher stability of Au NPs stabilized by I-8 alginate than that of I-1 alginate can be ascribed to the higher viscosity of I-8 alginate and its solution. This can help reduce the collision, settling, aggregation, and precipitation of Au NPs during preparation, drying, and redispersion.

3. CONCLUSIONS

In summary, alginate-stabilized Au NPs using MWPLP were prepared. The introduction of alginate could (1) accelerate the reaction rate, (2) prevent aggregation and precipitation due to long time discharge in MWPLP, and (3) provide long-term stability. The size of Au NPs prepared in different concentrations of alginate ranged from 41 to 12 nm, indicating that the concentration of alginate could be used for controlling the size of Au NPs. An abnormal size change (from large to small) that is opposite to the typical particle growth in the bottom-up chemical reduction was observed. A possible mechanism of the observed phenomenon was proposed based on dynamical and thermodynamical instability. The alginate dispersions with Au NPs were dried and redispersed to evaluate the effect of the drying and redispersion process on the Au NPs. Results suggest that the process had an imperceptible effect on the Au NPs in terms of their size and dispersibility. As a consequence, this strategy might be an effective technique for the long-term storage of Au NPs and other metal NPs. The stabilized Au NPs without the addition of toxic reducing or stabilizing agents can be appropriate for biomedical applications.

4. EXPERIMENTAL SECTION

4.1. Materials. Tetrachloroauric(III) acid hydrate ($HAuCl_4 \cdot nH_2O$, n = 3.7, Kojima, Japan) and sodium alginate (I-1 (molecular weight, 1.5×10^6) and I-8 (molecular weight, 3.2×10^6), Kimica Corp., Japan) were used as a precursor and an additive, respectively. All "alginate" described in this paper without indication is sodium alginate I-1. One gram of $HAuCl_4 \cdot nH_2O$ (n = 3.7) was dissolved in 100 mL of pure water to obtain 24.6 mM aqueous $HAuCl_4$. All chemicals were used as received. Pure water (Organo/ELGA Purelab system, >18.2 MΩ·cm) was used to prepare solutions for plasma reaction.

4.2. Apparatus. A schematic illustration of the homemade microwave-induced plasma apparatus with a reactor is shown in Scheme 1a. Microwave (2.45 GHz) was emitted from a magnetron (Micro Denshi UW-1500) and passed through a power meter, a tuner, a WRJ-2 rectangular waveguide (109.22 × 54.61 mm) to a coaxial adaptor, and a coaxial plasma source electrode. The coaxial electrode was attached in the middle of the waveguide, and its front was projected into the chamber. This electrode terminated with an Y_2O_3-coated stainless-steel tip. Contaminations from the electrode were suppressed using this ceramic-coated electrode, as this electrode material did not dissolve in the reaction solution during plasma ignition. The inside of a stainless-steel reactor (500 cm^3) was coated with PTFE. The plasma reaction solution was cooled using a stainless-steel cooling spiral containing chilled liquid at 0 °C. The reaction temperature was measured with a thermocouple. When the microwave output was fixed at 500 W, the reaction temperature was increased by plasma irradiation, reaching 33 °C after 3 min, and then remained at 33 °C for the duration of the irradiation. Plasma ignition and the solution during the plasma reaction can be observed by the eye through a quartz window. The pressure was decreased using a diaphragm vacuum pump and measured with a vacuum gauge.

4.3. Preparation of Gold Nanoparticles. The preparation route is illustrated in Scheme 1c. Aqueous sodium alginate solutions (0.5, 1.0, and 2.0% (w/v)) were prepared by dissolving 0.5, 1.0, and 2.0 g of sodium alginate into 100 mL of water, respectively. Aqueous $HAuCl_4$ solution (24.6 mM; 4.08 mL) was added into 195.92 mL of water to obtain 0.5 mM $HAuCl_4$ solution. The volume ratio of $HAuCl_4$ and alginate solution was 2:1. The mixed solution was stirred for 3 h for getting homogeneous solutions and then introduced into the reaction vessel. The prepared Au NPs were labeled with sodium alginate of different concentrations: 0.5, 1.0, and 2.0% (w/v). The microwave output was kept at 500 W during the reaction. The reaction lasted for 10, 20, 30, 40, 50, and 60 min for the pure water group (Au NPs prepared in pure water) and 10, 15, 20, and 25 min for sodium alginate groups (Au NPs prepared in alginate solutions).

4.4. Drying and Redispersion of Alginate-Stabilized Au NPs. After preparation, alginate-stabilized Au NP dispersions were concentrated by a rotary evaporator (Eyela N-1300, Tokyo Rikikai Co. Ltd.). Then, the concentrated alginate-stabilized Au NP dispersions were collected and transferred to a vacuum oven for further drying. For the redispersion of alginate-stabilized Au NPs, alginate-stabilized Au NPs were weighed and dispersed in DI water to the original concentrations.

4.5. Characterizations. The UV–Vis extinction spectra of the obtained Au NP dispersions were collected to observe Au NP formation at different times by using a UV–Vis spectrophotometer (Shimadzu UV-1800) and a quartz cell with a 1 cm optical path. During the plasma reaction, 3 mL of the sample solution was taken directly from the reaction vessel for each measurement at various reaction times. Transmission electron microscopy (TEM, JEOL JEM 2000-ES, at 200 kV) with energy dispersive X-ray spectroscopy (EDS) was used to analyze the morphology, size, and elemental composition of Au NPs. The X-ray diffraction (XRD) patterns were collected by using a Rigaku Miniflex II X-ray diffractometer. For TEM sample preparation, Au NP dispersion was dropped on collodion film-coated copper TEM grids and left to be naturally dried. The particle size and size distribution of

https://doi.org/10.1021/acsomega.1c06769
ACS Omega 2022, 7, 6238–6247

more than 100 Au NPs were measured from TEM images by ImageJ (available as freeware from http://rsbweb.nih.gov/ij/). Concentrations of Au NPs were determined by inductively coupled plasma atomic emission spectrometry (ICP-AES) using an ICPE-9000 (Shimadzu) spectrometer. Zeta potentials of Au NP dispersions were measured by the zeta potential and particle size analyzer ELSZ-2 (Photal Otsuka Electronics, Japan). pH values were collected by a pH meter D-55 (Horiba, Japan).

■ ASSOCIATED CONTENT

Supporting Information

The Supporting Information is available free of charge at https://pubs.acs.org/doi/10.1021/acsomega.1c06769.

> Size distributions of Au NPs prepared in alginate solutions with various conditions, image of Au NPs prepared in pure water to aggregate/precipitate with time, images of Au NPs prepared in different concentrations of alginate solutions, EDS results of Au aggregations, TEM image of Au aggregations, size changes of Au NPs prepared in alginate solutions with different reaction times, and images of Au NPs prepared in pure water (PDF)

■ AUTHOR INFORMATION

Corresponding Author

Tetsu Yonezawa − *Division of Materials Science and Engineering, Faculty of Engineering, Hokkaido University, Sapporo, Hokkaido 060-8628, Japan;* orcid.org/0000-0001-7371-204X; Email: tetsu@eng.hokudai.ac.jp

Authors

Haoran Liu − *Division of Materials Science and Engineering, Faculty of Engineering, Hokkaido University, Sapporo, Hokkaido 060-8628, Japan*

Kai Ikeda − *Division of Materials Science and Engineering, Faculty of Engineering, Hokkaido University, Sapporo, Hokkaido 060-8628, Japan*

Mai Thanh Nguyen − *Division of Materials Science and Engineering, Faculty of Engineering, Hokkaido University, Sapporo, Hokkaido 060-8628, Japan;* orcid.org/0000-0001-5436-123X

Susumu Sato − *Department of Information Systems, Faculty of Engineering, Saitama Institute of Technology, Fukaya, Saitama 369-0293, Japan*

Naoki Matsuda − *National Institute of Advanced Industrial Science and Technology (AIST), Tosu, Saga 841-0052, Japan*

Hiroki Tsukamoto − *Division of Materials Science and Engineering, Faculty of Engineering, Hokkaido University, Sapporo, Hokkaido 060-8628, Japan*

Tomoharu Tokunaga − *Department of Materials Science and Engineering, Faculty of Engineering, Nagoya University, Nagoya 464-8603, Japan*

Complete contact information is available at: https://pubs.acs.org/10.1021/acsomega.1c06769

Notes

The authors declare no competing financial interest.

■ ACKNOWLEDGMENTS

This work was partially supported by Hokkaido University. T.Y. also thanks the financial support by The Translational Research program; Strategic PRomotion for practical application of INovative medical Technology (TR-SPRINT) funded by The Japan Agency for Medical Research and Development (AMED) (Seeds A), Japan, and JKA Foundation Promotion fund from KEIRIN Race: 2021M-113. The authors thank Drs. Y. Ishida and S. Zhu (Hokkaido University) for fruitful discussions and experimental assistance. The authors thank Mr. T. Tanioka, Mr. R. Oota, Ms. R. Yokohira, and Ms. N. Hirai (Hokkaido University) for their assistance in TEM-EDS analysis. The authors thank the Open Facility, Global Facility Center, Creative Research Institution, Hokkaido University, for allowing us to analyze Au NPs using an ICPE-9000 (Shimadzu) and providing insight and expertise that greatly assisted the research. H.L. would like to thank the China Scholarship Council (CSC) for the financial support for his stay in Sapporo.

■ REFERENCES

(1) Sharifi, M.; Attar, F.; Saboury, A. A.; Akhtari, K.; Hooshmand, N.; Hasan, A.; El-Sayed, M. A.; Falahati, M. Plasmonic gold nanoparticles: Optical manipulation, imaging, drug delivery and therapy. *J. Controlled Release* **2019**, *311-312*, 170−189.

(2) Xi, D.; Dong, S.; Meng, X.; Lu, Q.; Meng, L.; Ye, J. Gold nanoparticles as computerized tomography (CT) contrast agents. *RSC Adv.* **2012**, *2*, 12515−12524.

(3) Hainfeld, J. F.; Slatkin, D. N.; Focella, T. M.; Smilowitz, H. M. Gold Nanoparticles: A New X-Ray Contrast Agent. *Br. J. Radiol.* **2006**, *79*, 248−253.

(4) Mahan, M. M.; Doiron, A. L. Gold Nanoparticles as X-ray, CT, and Multimodal Imaging Contrast Agents: Formulation, Targeting, and Methodology. *J. Nanomater.* **2018**, 5837276.

(5) Von Maltzahn, G.; Park, J.-H.; Lin, K. Y.; Singh, N.; Schwöppe, C.; Mesters, R.; Berdel, W. E.; Ruoslahti, E.; Sailor, M. J.; Bhatia, S. N. Nanoparticles that communicate in vivo to amplify tumour targeting. *Nat. Mater.* **2011**, *10*, 545−552.

(6) Popovtzer, R.; Agrawal, A.; Kotov, N. A.; Popovtzer, A.; Balter, J.; Carey, T. E.; Kopelman, R. argeted gold nanoparticles enable molecular CT imaging of cancer. *Nano Lett.* **2008**, *8*, 4593−4596.

(7) Liu, M.; Guyot-Sionnest, P.; Lee, T.-W.; Gray, S. K. Optical properties of rodlike and bipyramidal gold nanoparticles from three-dimensional computations. *Phys. Rev. B* **2007**, *76*, 235428.

(8) Lim, E.-K.; Kim, T.; Paik, S.; Haam, S.; Huh, Y.-M.; Lee, K. Nanomaterials for theranostics: recent advances and future challenges. *Chem. Rev.* **2015**, *115*, 327−394.

(9) Dykman, L.; Khlebtsov, N. Gold nanoparticles in biomedical applications: recent advances and perspectives. *Chem. Soc. Rev.* **2012**, *41*, 2256−2282.

(10) Toshima, N.; Harada, M.; Yamazaki, Y.; Asakura, K. Catalytic Activity and Structural Analysis of Polymer-Protected Au-Pd Bimetallic Clusters Prepared by the Simultaneous Reduction of $HAuCl_4$ and $PdCl_2$. *J. Phys. Chem.* **1992**, *96*, 9927−9933.

(11) Yonezawa, T.; Toshima, N. Polymer- and micelle-protected gold/platinum bimetallic systems. Preparation, application to catalysis for visible-light-induced hydrogen evolution, and analysis of formation process with optical methods. *J. Mol. Catal.* **1993**, *83*, 167−181.

(12) Li, C.; Shuford, K. L.; Chen, M.; Lee, E. J.; Cho, S. O. A Facile Polyol Route to Uniform Gold Octahedra with Tailorable Size and Their Optical Properties. *ACS Nano* **2008**, *2*, 1760−1769.

(13) Brust, M.; Walker, M.; Bethell, D.; Schiffrin, D. J.; Whyman, R. Synthesis of Thiol-derivatised Gold Nanoparticles in a Two-phase Liquid-Liquid System. *J. Chem. Soc., Chem. Commun.* **1994**, 801−802.

(14) Yonezawa, T.; Yasui, K.; Kimizuka, N. Controlled Formation of Smaller Gold Nanoparticles by the Use of Four-Chained Disulfide Stabilizer. *Langmuir* **2001**, *17*, 271−273.
(15) Huang, H.; Yang, X. Synthesis of polysaccharide-stabilized gold and silver nanoparticles: a green method. *Carbohydr. Res.* **2004**, *339*, 2627−2631.
(16) Nalawade, P.; Mukherjee, T.; Kapoor, S. Green synthesis of gold nanoparticles using glycerol as a reducing agent. *Adv. Nanopart.* **2013**, *2*, 31462.
(17) He, Y. Q.; Liu, S. P.; Kong, L.; Liu, Z. F. A study on the sizes and concentrations of gold nanoparticles by spectra of absorption, resonance Rayleigh scattering and resonance non-linear scattering. *Spectrochim. Acta, Part A* **2005**, *61*, 2861−2866.
(18) Nishimoto, M.; Yonezawa, T.; Čempel, D.; Nguyen, M. T.; Ishida, Y.; Tsukamoto, H. Effect of H_2O_2 on Au nanoparticle preparation using microwave-induced plasma in liquid. *Mater. Chem. Phys.* **2017**, *193*, 7−12.
(19) Matsuda, N.; Nakashima, T.; Okabe, H.; Yamada, H.; Shiroishi, H.; Nagamura, T. Preparation of Au nano-particle dispersed water solution without surfactant for surface-enhanced Raman scattering platform. *Mol. Cryst. Liq. Cryst.* **2017**, *653*, 137−143.
(20) Matsuda, N.; Okabe, H.; Nagamura, T.; Uehara, M. Possible application of gold thin films formed from surfactant free gold nano-particle dispersed in aqueous solutions to surface-enhanced Raman scattering spectroscopy. *Mol. Cryst. Liq. Cryst.* **2019**, *686*, 63−69.
(21) Čempel, D.; Nguyen, M. T.; Ishida, Y.; Yonezawa, T. l-Arginine-Stabilized Highly Uniform Ag Nanoparticles Prepared in a Microwave-Induced Plasma-in-Liquid Process (MWPLP). *Bull. Chem. Soc. Jpn.* **2018**, *91*, 362−367.
(22) Sato, S.; Mori, K.; Ariyada, O.; Atsushi, H.; Yonezawa, T. Synthesis of nanoparticles of silver and platinum by microwave-induced plasma in liquid. *Surf. Coat. Technol.* **2011**, *206*, 955−958.
(23) Nishimoto, M.; Tsukamoto, H.; Nguyen, M. T.; Yonezawa, T. Effects of Additives on the Preparation of Ag Nanoparticles Using the Microwave-Induced Plasma in Liquid Process. *ChemistrySelect* **2017**, *2*, 7873−7879.
(24) Čempel, D.; Nguyen, M. T.; Ishida, Y.; Tokunaga, T.; Yonezawa, T. Ligand free green plasma-in-liquid synthesis of Au/Ag Alloy nanoparticles. *New J. Chem.* **2018**, *42*, 5680−5687.
(25) Čempel, D.; Nguyen, M. T.; Ishida, Y.; Tsukamoto, H.; Shirai, H.; Wang, Y.; Wu, W.-C.; Yonezwa, T. Au nanoparticles prepared using a coated electrode in plasma-in-liquid process: effect of the solution pH. *J. Nanosci. Nanotechnol.* **2016**, *16*, 9257−9262.
(26) Szabó, D. V.; Schlabach, S. Microwave plasma synthesis of materials-From physics and chemistry to nanoparticles: A materials scientist's viewpoint. *Inorganics* **2014**, *2*, 468−507.
(27) Mukasa, S.; Nomura, S.; Toyota, H. Observation of microwave in-liquid plasma using high-speed camera. *Jpn. J. Appl. Phys.* **2007**, *46*, 6015.
(28) Yonezawa, T.; Čempel, D.; Nguyen, M. T. Microwave-induced plasma-in-liquid process for nanoparticle production. *Bull. Chem. Soc. Jpn.* **2018**, *91*, 1781−1798.
(29) Patel, J.; Němcová, L.; Maguire, P.; Graham, W.; Mariotti, D. Synthesis of surfactant-free electrostatically stabilized gold nano-particles by plasma-induced liquid chemistry. *Nanotechnology* **2013**, *24*, 245604.
(30) Zhao, X.; Xia, Y.; Li, Q.; Ma, X.; Quan, F.; Geng, C.; Han, Z. Microwave-assisted synthesis of silver nanoparticles using sodium alginate and their antibacterial activity. *Colloids Surf., A* **2014**, *444*, 180−188.
(31) Watthanaphanit, A.; Panomsuwan, G.; Saito, N. A novel one-step synthesis of gold nanoparticles in an alginate gel matrix by solution plasma sputtering. *RSC Adv.* **2014**, *4*, 1622−1629.
(32) Jin, B.; Sushko, M. L.; Liu, Z.; Jin, C.; Tang, R. In situ liquid cell TEM reveals bridge-induced contact and fusion of Au nanocrystals in aqueous solution. *Nano Lett.* **2018**, *18*, 6551−6556.
(33) Aabdin, Z.; Lu, J.; Zhu, X.; Anand, U.; Loh, N. D.; Su, H.; Mirsaidov, U. Bonding pathways of gold nanocrystals in solution. *Nano Lett.* **2014**, *14*, 6639−6643.
(34) Gao, X.; Zhang, Y.; Zhao, Y. Biosorption and reduction of Au (III) to gold nanoparticles by thiourea modified alginate. *Carbohydr. Polym.* **2017**, *159*, 108−115.
(35) De Jong, W. H.; Hagens, W. I.; Krystek, P.; Burger, M. C.; Sips, A. J. A. M.; Geertsma, R. E. Particle size-dependent organ distribution of gold nanoparticles after intravenous administration. *Biomaterials* **2008**, *29*, 1912−1919.
(36) Cho, W.-S.; Cho, M.; Jeong, J.; Choi, M.; Han, B. S.; Shin, H.-S.; Hong, J.; Chung, B. H.; Jeong, J.; Cho, M.-H. Size-dependent tissue kinetics of PEG-coated gold nanoparticles. *Toxicol. Appl. Pharmacol.* **2010**, *245*, 116−123.
(37) Woźniak, A.; Malankowska, A.; Nowaczyk, G.; Grześkowiak, B. F.; Tuśnio, K.; Słomski, R.; Zaleska-Medynska, A.; Jurga, S. Size and shape-dependent cytotoxicity profile of gold nanoparticles for biomedical applications. *J. Mater. Sci.: Mater. Med.* **2017**, *28*, 92.
(38) Zhang, X.-D.; Wu, D.; Shen, X.; Chen, J.; Sun, Y.-M.; Liu, P.-X.; Liang, X.-J. Size-dependent radiosensitization of PEG-coated gold nanoparticles for cancer radiation therapy. *Biomaterials* **2012**, *33*, 6408−6419.
(39) Valdez, J.; Gómez, I. One-step green synthesis of metallic nanoparticles using sodium alginate. *J. Nanomater.* **2016**, 9790345.
(40) Jabbareh, M. A. Size, shape and temperature dependent surface energy of binary alloy nanoparticles. *Appl. Surf. Sci.* **2017**, *426*, 1094−1099.
(41) Bhumkar, D. R.; Joshi, H. M.; Sastry, M.; Pokharkar, V. B. Chitosan reduced gold nanoparticles as novel carriers for trans-mucosal delivery of insulin. *Pharm. Res.* **2007**, *24*, 1415−1426.
(42) Guo, R.; Wang, H.; Peng, C.; Shen, M.; Pan, M.; Cao, X.; Zhang, G.; Shi, X. X-ray attenuation property of dendrimer-entrapped gold nanoparticles. *J. Phys. Chem. C* **2010**, *114*, 50−56.
(43) Liu, H.; Wang, H.; Guo, R.; Cao, X.; Zhao, J.; Luo, Y.; Shen, M.; Zhang, G.; Shi, X. Size-controlled synthesis of dendrimer-stabilized silver nanoparticles for X-ray computed tomography imaging applications. *Polym. Chem.* **2010**, *1*, 1677−1683.
(44) Gupta, A.; Moyano, D. F.; Parnsubsakul, A.; Papadopoulos, A.; Wang, L.-S.; Landis, R. F.; Das, R.; Rotello, V. M. Ultrastable and biofunctionalizable gold nanoparticles. *ACS Appl. Mater. Interfaces* **2016**, *8*, 14096−14101.
(45) Abdelwahed, W.; Degobert, G.; Stainmesse, S.; Fessi, H. Freeze-drying of nanoparticles: formulation, process and storage considerations. *Adv. Drug Delivery Rev.* **2006**, *58*, 1688−1713.
(46) Sharma, D. A biologically friendly single step method for gold nanoparticle formation. *Colloids Surf., B* **2011**, *85*, 330−337.
(47) Ortiz, M.; Fragoso, A.; O'Sullivan, C. K. Detection of antigliadin autoantibodies in celiac patient samples using a cyclodextrin-based supramolecular biosensor. *Anal. Chem.* **2011**, *83*, 2931−2938.
(48) Gao, J.; Huang, X.; Liu, H.; Zan, F.; Ren, J. Colloidal stability of gold nanoparticles modified with thiol compounds: bioconjugation and application in cancer cell imaging. *Langmuir* **2012**, *28*, 4464−4471.
(49) Fang, C.; Bhattarai, N.; Sun, C.; Zhang, M. Functionalized nanoparticles with long-term stability in biological media. *Small* **2009**, *5*, 1637−1641.

https://doi.org/10.1021/acsomega.1c06769
ACS Omega 2022, 7, 6238−6247